



Publication Year	2002
Acceptance in OA @INAF	2023-02-03T15:18:18Z
Title	Ultraviolet properties of primeval galaxies: Theoretical models from stellar population synthesis
Authors	BUZZONI, Alberto
DOI	10.1086/338896
Handle	http://hdl.handle.net/20.500.12386/33144
Journal	THE ASTRONOMICAL JOURNAL
Number	123

ULTRAVIOLET PROPERTIES OF PRIMEVAL GALAXIES: THEORETICAL MODELS FROM STELLAR POPULATION SYNTHESIS

ALBERTO BUZZONI

Telescopio Nazionale Galileo, Apdo. Postal 565, E-38700 Santa Cruz de La Palma, Spain; and Osservatorio Astronomico di Brera, I-20121 Milano, Italy;
buzzoni@tng.iac.es

Received 2001 June 18; accepted 2001 November 29

ABSTRACT

The ultraviolet luminosity evolution of star-forming galaxies is explored from the theoretical point of view, especially focusing on the theory of UV energetics in simple and composite stellar populations and its relationship to the star formation rate and other main evolutionary parameters. Galaxy emission below $\lambda < 3000 \text{ \AA}$ directly correlates with actual star formation, not depending on the total mass of the system. A straightforward calibration is obtained, in this sense, from the theoretical models at 1600, 2000, and 2800 \AA , and a full comparison is carried out with *IUE* data and other balloon-borne observations for local galaxies. The claimed role of late-type systems as prevailing contributors to the cosmic UV background is reinforced by our results; at 2000 \AA , Im irregulars are found in fact nearly 4 orders of magnitude brighter than ellipticals, per unit luminous mass. The role of dust absorption in the observation of high-redshift galaxies is assessed, comparing the model output and observed spectral energy distribution of local galaxy samples. Similar to what we observe in our own galaxy, a quick evolution in the dust environment might be envisaged in primeval galaxies, with an increasing fraction of luminous matter that would escape the regions of harder and “clumpy” dust absorption on a timescale of some 10^7 yr, comparable to the lifetime of stars of 5–10 M_{\odot} .

Key words: dust, extinction — galaxies: evolution — galaxies: starburst — galaxies: stellar content — ultraviolet emission

In ricordo di mio padre, per tutto il bene che mi ha dato.

1. INTRODUCTION

The recent major improvements in the observation of the deep universe, with both the *Hubble Space Telescope (HST)* and ground-based telescopes of the new generation, has greatly increased our chances to probe the cosmological model by venturing to search for primeval galaxies. When observing in the optical or infrared range, however, we are probing rest-frame ultraviolet (UV) emission of high-redshift objects, and we should therefore rely on confident recognition criteria in this wavelength range in order to pick up distant galaxies and track their evolution back in time.

Because of atmosphere opacity, nearby galaxies are still poorly explored in the extreme-UV range, and their data cannot fully match high- z observations (Lanzetta, Yahil, & Fernández-Soto 1996; Massarotti, Iovino, & Buzzoni 2001a). In any case, such an empirical approach would neglect evolution, while sample selection and Malmquist bias could give rise to a misleading interpretation of the high-redshift data (Buzzoni 1998, 2001; Adelberger & Steidel 2000). For all these reasons, galaxy models may prove to be a more effective tool for matching primeval galaxy evolution, although within the limits of the established theoretical scenario.

The observation of UV emission of star-forming galaxies at cosmological distances, in the Hubble Deep Field (Williams et al. 1996) or in other deep surveys (Lilly et al. 1996; Connolly et al. 1997), has recently led to important advances in the study of cosmic star formation (Madau, Pozzetti, & Dickinson 1998; Steidel et al. 1999; Massarotti et al. 2001b), fueling the current debate on the epoch of galaxy formation. In light of these results, in this work my aim is to assess in more detail the expected UV properties of primeval galaxies. In particular, I focus on the theory of UV ener-

getics in stellar populations, in order to explore its dependence on the star formation rate (SFR) and other main evolutionary parameters. This will rely on a previous (Buzzoni 1989, 1995, 1998) theoretical framework for evolutionary population synthesis. To some extent, my analysis is complementary to the work of Leitherer et al. (1999), as I track here late evolution of star-forming galaxies, when morphology begins to differentiate late- and early-type systems along the Hubble sequence.

My discussion will first consider, in § 2, the UV evolution of a simple stellar population (SSP). This will provide the basic theoretical tools to derive an absolute calibration of galaxy UV luminosity and actual SFR, and to study its possible dependence on metallicity. A possible scheme for the spectral evolution of star-forming galaxies of different morphological type is outlined in § 3, where I compute a new set of synthesis models and compare, in § 4, the theoretical output with *IUE* observations and other UV data available for local galaxies. The problem of dust absorption is also reviewed in the latter section, discussing its possible impact on the evolutionary scenario of high-redshift galaxies. Relevant conclusions are finally summarized in § 5.

2. FUNDAMENTALS OF UV LUMINOSITY IN STELLAR POPULATIONS

Contrary to the case of optical and infrared evolution, the ultraviolet luminosity of star-forming galaxies is largely dominated by short-lived stars of high mass (Kennicutt 1998). This makes population synthesis models much simpler, because hot main-sequence (MS) stars are the prevailing contributors to the galaxy energetic budget at short wavelengths. In a more refined analysis, however, the input from low-mass stars ($M \lesssim 1 M_{\odot}$) should also be conven-

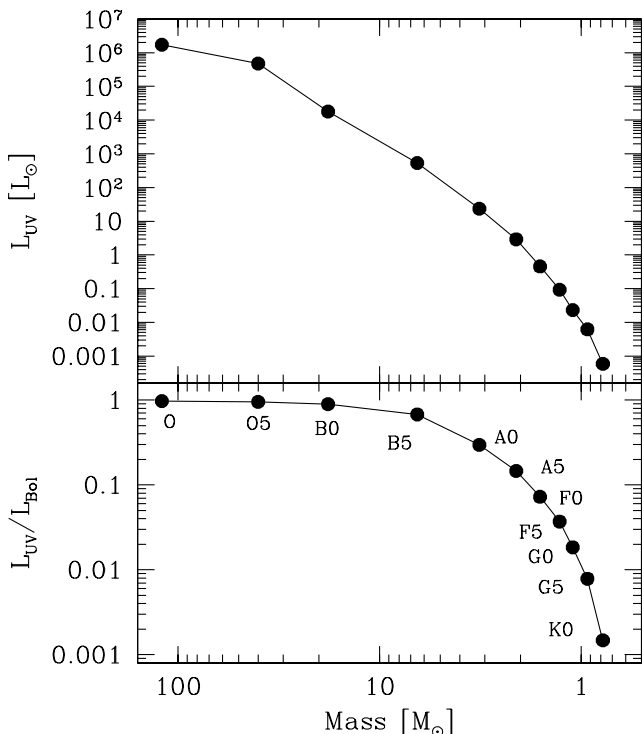


FIG. 1.—UV L - M relation for MS stars (MK class V). The top panel reports the emission for $\lambda < 3000 \text{ \AA}$, in bolometric solar units. The relative fraction of ultraviolet to bolometric is displayed in the bottom panel. Kurucz' (1992) model atmospheres have been used to compute synthetic spectra. The calibration for the $120 M_{\odot}$ star is from Bressan et al. (1993).

iently sized up, since these stars smoothly cumulate over the entire galaxy life and could reach hot temperatures at some stage of the post-MS evolution. The SSP theory (Renzini & Buzzoni 1986; Buzzoni 1989) provides an effective tool to consistently assess the general UV properties of stellar populations. As we will see, the relevant results for the SSP case can also easily apply to the study of star-forming galaxies.

An illustrative summary of the integrated luminosity emitted shortward of 3000 \AA by MS stars of different spectral type is reported in Figure 1. The plot is based on the Kurucz (1992) model atmospheres, adopting a standard temperature-luminosity-mass calibration for class V stars of solar metallicity as from Allen (1973, p. 209).¹ One sees from the figure that at least half the bolometric luminosity of stars more massive than $\sim 5 M_{\odot}$ is spent in the ultraviolet. For stars earlier than F0 ($M \gtrsim 2 M_{\odot}$), a simple L - M calibration can be derived, such as $L_{UV} = KM^{\alpha}$, with $(K, \alpha) = (0.21, 4.0)$ for $\lambda < 3000 \text{ \AA}$ (expressing both L and M in solar units). At lower mass, the slope of the relation quickly steepens, and the UV contribution drops to nominal values for K stars.

As far as a SSP is concerned, with stars distributed in mass according to a power-law initial mass function (IMF) such as $dN = AM^{-s}dM$ ($s = 2.35$ for the Salpeter standard

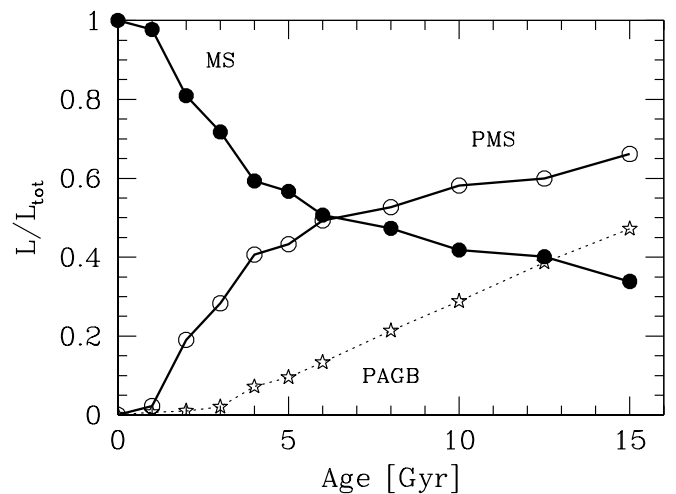


FIG. 2.—SSP luminosity evolution in the UV wavelength range ($\lambda < 3000 \text{ \AA}$) according to Buzzoni's (1989) synthesis code. A solar metallicity and a Salpeter IMF are assumed. The relative contribution from MS (filled circles) and post-MS (open circles) stars is compared. The luminosity fraction provided by post-AGB stars alone (stars) is also singled out.

case), the integrated MS luminosity results:

$$L_{MS} = AK \int_{M_l}^{M_{TO}} m^{\alpha-s} dm, \quad (1)$$

where A is a normalization factor that scales with the SSP total mass, while M_l is the lower limit for the IMF. The integral is constrained by the mass of the turnoff (TO) stars (M_{TO}) that leave the MS. This actually marks the “clock” of the SSP, giving the time dependence of L_{MS} . Recalling that $L_{TO} = KM_{TO}^{\alpha}$, and provided that $s < (1 + \alpha)$ and $M_{TO} \gg M_l$, after some appropriate substitutions we have

$$L_{MS} = \frac{A}{1 + \alpha - s} M_{TO}^{1-s} L_{TO}. \quad (2)$$

Equation (2) simply relates the total MS luminosity to the TO luminosity of the evolving stars in the SSP.

Detailed SSP evolution for $\lambda < 3000 \text{ \AA}$ is computed in Figure 2, where I extend to younger ages the original model sequence of Buzzoni (1989) for a Salpeter IMF and solar metallicity. In this figure I also single out the contribution from post-AGB stars experiencing the planetary nebula event for $t \gtrsim 1$ Gyr. As is well known, post-AGB stars are important contributors to short-wavelength luminosity in old SSPs, and may actually constrain the ultraviolet properties of present-day elliptical galaxies (Renzini & Buzzoni 1986; Burstein et al. 1988; Greggio & Renzini 1990; Yi et al. 1999). The SSP model of Figure 2 assumes a red horizontal branch (HB) morphology; my choice relies on the fact that HB evolution quickly turns to redder colors with increasing star mass and/or metallicity. Although stars with temperatures in excess of 10,000 K are recognized in some old metal-poor Galactic globular clusters (Cacciari et al. 1995), a red HB is always to be expected at younger ages (i.e., for $t \lesssim 12$ Gyr; cf. Fig. 4 of Buzzoni 1989).

The resulting SSP luminosity evolution at three reference wavelength values, namely, 1600, 2000, and 2800 \AA , is reported in Table 1 for a Salpeter IMF with an upper cutoff mass of $120 M_{\odot}$.

¹ Allen's (1973) classical compilation for MS stellar parameters is also a suitable match to more sophisticated theoretical calibrations, such as, e.g., those deriving from the Padova (Bressan et al. 1993) and Geneva (Schaller et al. 1992) stellar tracks.

TABLE 1
SSP ULTRAVIOLET EVOLUTION

AGE (Gyr)	$\Delta \log L$		
	1600 Å	2000 Å	2800 Å
0.003	0.00	0.00	0.00
0.013	-2.13	-1.94	-1.76
0.024	-2.49	-2.27	-2.06
0.046	-2.85	-2.60	-2.35
0.057	-2.96	-2.70	-2.44
0.078	-3.13	-2.85	-2.58
0.10	-3.27	-2.96	-2.68
0.20	-3.66	-3.29	-2.97
0.40	-4.26	-3.69	-3.30
0.60	-4.94	-4.00	-3.52
0.80	-5.47	-4.34	-3.73
1.0	-5.87	-4.64	-3.89
2.0	-7.04	-5.51	-4.37
4.0	-7.90	-6.23	-4.68
5.0	-8.02	-6.39	-4.78
6.0	-8.03	-6.56	-4.88
8.0	-8.03	-6.85	-5.05
10.0	-8.00	-7.11	-5.19
12.5	-7.88	-7.27	-5.32
15.0	-7.77	-7.37	-5.43

NOTE.—For a Salpeter IMF with upper cutoff mass of $120 M_{\odot}$.

2.1. UV Luminosity and SFR

Insofar as the MS contribution is the prevailing one in the UV energetic budget, the SSP luminosity evolution can be approximated by a simple analytical relation linking equation (2) with the theoretical stellar clock. The MS lifetime for stars in the different ranges of mass and solar metallicity can be evaluated from a number of sets of theoretical models. I considered the work of Becker (1981), Vandenberg (1985), Castellani, Chieffi, & Straniero (1990), Lattanzio (1991), Schaller et al. (1992), and Bressan et al. (1993). A useful fit to these data, which spans the whole range of mass, is

$$\log t = 0.825 \log^2(M_{\text{TO}}/120) + 6.43 \quad (3)$$

(cf. Fig. 3).

By differentiating equations (2) and (3) we obtain $d \log L_{\text{MS}} = (1 + \alpha - s)d \log M_{\text{TO}}$ and $d \log t = 1.65 \log(M_{\text{TO}}/120)d \log M_{\text{TO}}$, respectively. Assuming that $L_{\text{MS}} \equiv L_{\text{SSP}}$, this leads to

$$L_{\text{SSP}} \propto t^{0.6(1+\alpha-s)/\log(M_{\text{TO}}/120)} \equiv t^{-\gamma}. \quad (4)$$

The power index γ depends on M_{TO} and α , so that it slightly changes with time and wavelength (SSP luminosity fades more rapidly at shorter wavelength), but, as a general case, we could verify from Table 1 that $\gamma \geq 1$ for $\lambda < 3000 \text{ \AA}$. This feature has important consequences when linking UV luminosity and galaxy SFR. In the case of a star-forming galaxy with constant SFR, for example, actual luminosity simply follows as

$$L_{\text{gal}} \propto \text{SFR} \int_{t_{\text{min}}}^{t_{\text{gal}}} \tau^{-\gamma} d\tau \propto (\text{SFR } t_{\text{min}}) L_{t_{\text{min}}}^{\text{SSP}}, \quad (5)$$

where t_{gal} is the age of the system, and t_{min} is the lifetime of

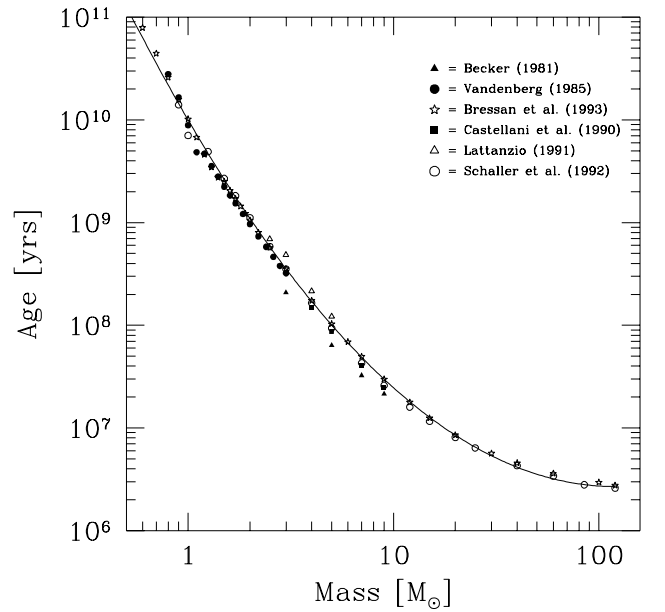


FIG. 3.—Theoretical MS lifetime vs. stellar mass for Z_{\odot} according to the evolutionary tracks by Becker (1981), Vandenberg (1985), Castellani et al. (1990), Lattanzio (1991), Schaller et al. (1992), and Bressan et al. (1993). The solid line is a fit to the data according to eq. (3).

the most massive stars in the IMF. The previous equation confirms that galaxy UV luminosity eventually does not depend on age, but only on its actual SFR (Kennicutt 1998; cf. his Fig. 2).

As a consequence, a *minimum* UV luminosity is reached by a star-forming galaxy that is the luminosity of a SSP of total mass $M_{\text{tot}} = \text{SFR } t_{\text{min}}$, where t_{min} comes from equation (3) once entering the upper stellar mass of the IMF (M_{up}). A straightforward relation exists between M_{tot} and the SSP scale factor A in equation (2) (cf. e.g., eq. [3] in Buzzoni 1989); making the relevant substitutions, we can write

$$\log L_{\text{min}} = \log \phi + \log \text{SFR}, \quad (6)$$

with

$$\phi = t_{\text{min}} \frac{|2-s|}{(1+\alpha-s)} \left(\frac{M_{\text{up}}}{M_{\text{cut}}} \right)^{2-s} \left(\frac{L_{\text{up}}}{M_{\text{up}}} \right). \quad (7)$$

In the previous equation, $M_{\text{cut}} = M_l$ if $s > 2$ and $M_{\text{cut}} = M_{\text{up}}$ if $s < 2$, while L_{up} is the TO luminosity of stars of mass M_{up} .

The expected L_{UV} versus SFR calibration at 2800 \AA is shown in Figure 4; a fairly good agreement is found with the Madau et al. (1998) results. As L_{UV} tracks the SFR via the relative number of high-mass stars, any nonstandard IMF could easily be accounted for. For example, a Scalo (1986) mass distribution would closely resemble in Figure 4 the case of a power-law IMF with $s \sim 2.5$. Table 2 reports the values of $\log \phi$ at 1600, 2000, and 2800 \AA for different IMF slopes around the Salpeter value.

2.2. Metallicity Effects

Since metal enrichment is a direct by-product of star formation, one would expect primordial galaxies to be essentially metal-poor aggregates. For this reason, it is also relevant to assess the validity of our L_{UV} versus SFR cali-

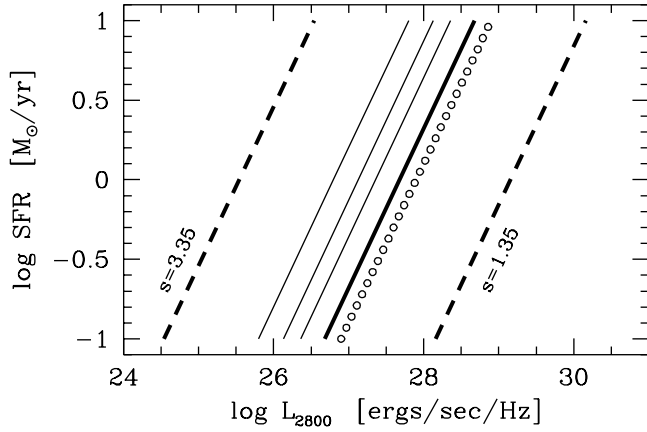


FIG. 4.—Theoretical L_{UV} vs. SFR calibration at 2800 Å according to eq. (6). Solid lines (left to right) refer to a Salpeter IMF ($s = 2.35$) and $M_{up} = 40, 60, 80,$ and $120 M_{\odot}$, with the last case marked in boldface. The IMF slopes for $s = 3.35$ and 1.35 and $M_{up} = 120 M_{\odot}$ are shown by the two dashed lines. The Madau et al. (1998) calibration for a Salpeter IMF and $M_{up} = 125 M_{\odot}$ is also given for comparison (dotted line).

bration in the case of a nonsolar evolutionary scenario with $Z \ll Z_{\odot}$. A change in metallicity would basically affect the MS fuel consumption, modulating the ϕ scaling factor in equation (6) via the term $L_{up}t_{min}$.

This point is explored in Figure 5, in which I compute the equivalent quantity $\text{fuel} = L_{ZAMS}t_{MS}$ from the Padova (Bressan et al. 1993; Fagotto et al. 1994) and Geneva (Schaller et al. 1992) stellar tracks, and study its absolute and relative variation with changing Z . In the top panel of the figure, the fraction of initial stellar mass burnt during MS evolution is reported for the model sequences at solar metallicity and the corresponding metal-poor ones (namely, $Z = 0.001$ for the Geneva tracks and $Z = 0.004$ for the Padova tracks). Compared with the Z_{\odot} case, metal-poor stars increase their MS lifetime but decrease bolometric (and UV) luminosity (cf. bottom panel). The two effects tend to nearly compensate, so that the factor $L_{up}t_{min}$

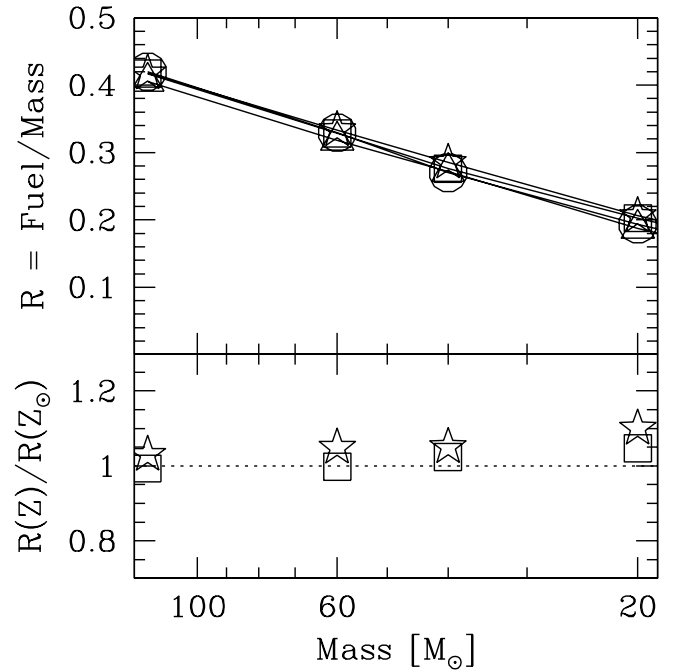


FIG. 5.—Top panel: Fraction of (initial) stellar mass consumed during MS evolution according to the Padova (Bressan et al. 1993; Fagotto et al. 1994) and Geneva (Schaller et al. 1992) evolutionary tracks. The plotted quantity is $R = \text{fuel}/\text{mass}$ where $\text{fuel} = (L_{ZAMS}t_{MS})/(0.007c^2)$ converted to hydrogen-equivalent solar masses. Padova tracks are for Z_{\odot} (open triangles) and $Z = 0.004$ (stars), while Geneva tracks are for Z_{\odot} (open circles) and $Z = 0.001$ (open squares). Bottom panel: Relative change in MS fuel consumption for the Padova $Z = 0.004$ tracks with respect to the solar case (stars) and, similarly, for the Geneva $Z = 0.001$ tracks (open squares).

remains almost constant over a wide range of stellar mass. This secures our L_{UV} versus SFR calibration within just a $\pm 10\%$ uncertainty even for quite extreme deviations from the solar metallicity.

2.3. Actual and Integrated Star Formation

Relying on equation (6), a convenient way to parameterize the luminosity evolution of a star-forming galaxy is

$$\log L_{gal}(t) = \log \phi + \log \text{SFR}(t) + \log Q(t) . \quad (8)$$

In addition to the contribution of fresh star formation, the correcting factor $Q(t)$ in this equation takes into account the “extra” luminosity contributed by the bulk of unevolved low-mass stars that have been accumulating along the galaxy’s life. It is interesting to theoretically evaluate this term in order to assess its real impact on galaxy spectral energy distribution (SED) for different star formation histories.

In its general case, the total luminosity of a star-forming galaxy can be computed as a suitable convolution of SSP “building blocks” with the SFR at the different epochs:

$$L_{gal}(t) = \int_{t_{min}}^t L_{SSP}(\tau) \text{SFR}(t - \tau) d\tau . \quad (9)$$

Once L_{gal} is obtained from equation (9), and L_{min} from equation (6), the Q residual luminosity simply derives from equation (8). For the present experiment, it is useful to consider the case of a power-law time decay such as $\text{SFR} \propto t^{-\eta}$. The major advantage of this simple parameterization is that

TABLE 2

THE $\log \phi$ CALIBRATION FOR STAR-FORMING GALAXIES

Wavelength (Å)	M_{up}			
	$120 M_{\odot}$	$80 M_{\odot}$	$60 M_{\odot}$	$40 M_{\odot}$
$s = 3.35$				
1600	25.77	25.62	25.51	25.36
2000	25.71	25.56	25.45	25.30
2800	25.54	25.39	25.28	25.13
$s = 2.35$				
1600	27.92	27.60	27.37	27.04
2000	27.86	27.54	27.31	26.98
2800	27.68	27.36	27.13	26.80
$s = 1.35$				
1600	29.39	28.89	28.53	28.03
2000	29.33	28.83	28.47	27.97
2800	29.16	28.66	28.30	27.80

NOTE.—The listed quantity is $\log L_{min}$ in $\text{ergs s}^{-1} \text{Hz}^{-1}$ according to eq. (6) for a $\text{SFR} = 1 M_{\odot} \text{yr}^{-1}$.

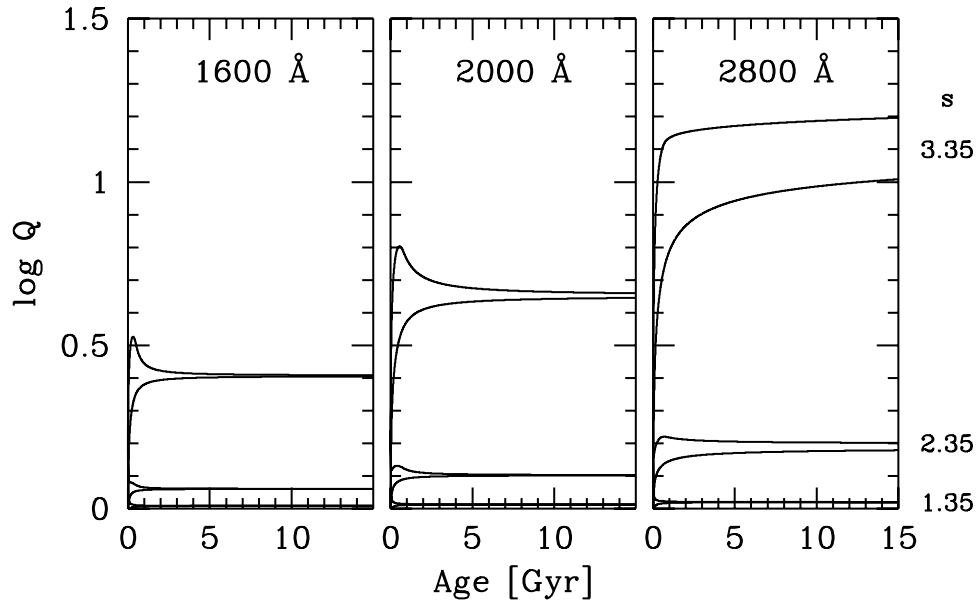


FIG. 6.— Q residual luminosity from the bulk of unevolved stars, after eq. (8), for different IMF power-law slopes with $s = 1.35, 2.35,$ and 3.35 , as labeled on the plots. Each set of curves provides the envelope for a $\text{SFR} \propto t^{-\eta}$ assuming η in the range $+0.8$ (upper envelope) and -0.8 (lower envelope). An upper IMF cutoff mass of $120 M_{\odot}$ is adopted.

it can easily account for a wide range of star formation histories in terms of an age-independent² distinctive birthrate

$$b = \text{SFR} / \langle \text{SFR} \rangle = (1 - \eta). \quad (10)$$

The value of η can be tuned up in order to reproduce galaxy colors at the present time. For a Salpeter IMF with stars between 0.1 and $120 M_{\odot}$, its allowed range is ± 0.8 (cf. § 3). With these assumptions, the resulting Q correction is summarized in Figure 6.

After a sharp increase on a few t_{\min} timescale, $\log Q$ tends to flatten and proceed steadily over the whole galaxy life. As expected, the luminosity correction becomes more important at longer wavelengths, and for a dwarf-dominated IMF (i.e., $s \gg 2.35$). However, for a Salpeter IMF, and even at 2800 \AA , its value is less than ~ 0.2 dex, confirming that UV luminosity of star-forming galaxies is only marginally modulated by the past star formation history. When moving to shorter wavelengths, equation (6) always tends to a fair estimate of galaxy total luminosity, and the SED will closely resemble that of the hottest composing stars (as $L_{\min} \propto L_{\text{up}}$ in the equation).

3. ULTRAVIOLET VERSUS OPTICAL LUMINOSITY

As I showed in previous section, past star formation history is better traced by the galaxy SED at longer wavelengths. Combining ultraviolet and optical observations, such as, for example, in the B and V bands, could therefore set valuable constraints on the stellar birthrate for galaxies along the whole Hubble morphological sequence (Larson & Tinsley 1978).

² At age t , $\text{SFR} = Ct^{-\eta}$, and its time average is $\langle \text{SFR} \rangle = Ct^{-1} \int_0^t \tau^{-\eta} d\tau$. Provided that $\eta < 1$, we always have $\langle \text{SFR} \rangle = \text{SFR} / (1 - \eta)$, from which the value of b directly follows, by definition.

3.1. The Galaxy Synthesis Models

To further investigate this important issue, this section introduces a simple family of galaxy models consisting of a spheroid and disk stellar component. Apart from minor details, this is basically the set of templates adopted by Massarotti et al. (2001a, 2001b, 2001c) for their study of the photometric redshift distribution in the Hubble Deep Field. The reader is also referred to these works of Massarotti et al. for a full comparison of the present theoretical framework with the codes of Bruzual & Charlot (1993) and Fioc & Rocca-Volmerange (1997), extensively used in recent extragalactic studies (see also Buzzoni 1998 for an in-depth discussion in the context of high-redshift observations). Here I particularly address the relevant UV features of the present theoretical output in the specific context of this discussion; the complete data set is also available in electronic form at the author's Web site.³

A major advantage of our theoretical approach over the previous synthesis codes (with perhaps the only relevant exception of the Arimoto & Jablonka 1991 models) resides in the fact that galaxy photometric evolution here comes as a result of the *individual* evolution of the disk and bulge sub-systems. As a general trend, disk luminosity is expected to slowly increase with time (because low-mass stars are “secularly” cumulating in a galaxy), as opposed to those in the bulge, which will fade because of an increasing fraction of dead stars (Renzini & Buzzoni 1986). Galaxy evolution back in time therefore results from the actual balance of these two different photometric trends; as a consequence, one single SFR characteristic timescale, as usually assumed in other synthesis codes, may not be an adequate description of the system as a whole.

Luminosity partition between the two basic building blocks of our synthesis models (i.e., disk and spheroid components) has been set empirically, relying on the Kent

³ Available at: <http://www.merate.mi.astro.it/~eps/home.html>.

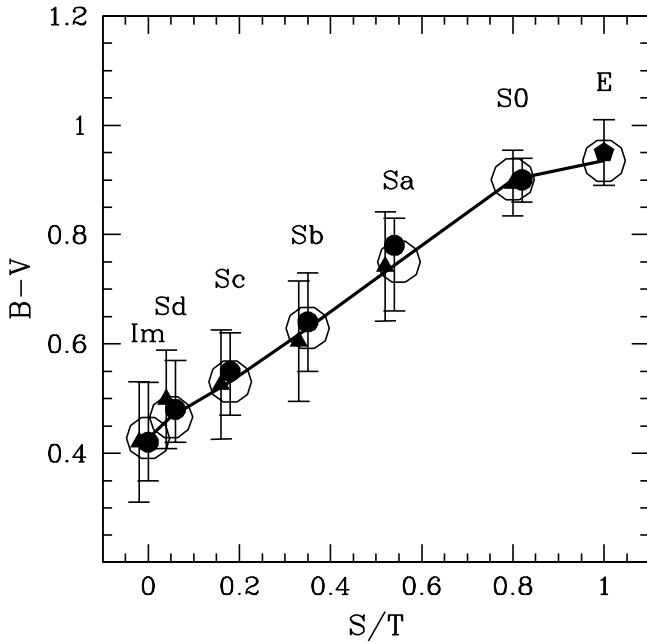


Fig. 7.—Theoretical colors for template galaxies of different morphological type, according to Table 3 (*large open circles*), compared with the mean $B-V$ locus from Roberts & Haynes (1994) (*filled circles*) and Buta et al. (1994) (*filled triangles*). Present-day galaxies are assumed to be 15 Gyr old. Data for ellipticals are from Buzzoni (1995).

(1985) galaxy decomposition profiles. These observations have been carried out in the Gunn r band and also provide a confident estimate of the bolometric partition (Buzzoni 1989). From these data, for each Hubble type I calibrated a bolometric morphological parameter defined as $S/T = L(\text{spheroid})/L(\text{tot})$. According to the observations, the luminous mass of the disk remains roughly constant along the S0 \rightarrow Im sequence, while the bulge luminosity decreases in later type spirals (Arimoto & Jablonka 1991; Gavazzi 1993).

For the spheroid subsystem, a SSP evolution with solar metallicity has been adopted, according to Buzzoni (1989, 1995). Disk SFR is in the form of a power law, as discussed in the previous section, with stars between 0.1 and 120 M_{\odot} according to a Salpeter IMF. Luminosity of the disk subsystem can be computed via equation (5), in which I tune up the SFR index η so as to reproduce the $B-V$ color of present-day galaxies along the whole Hubble sequence. The

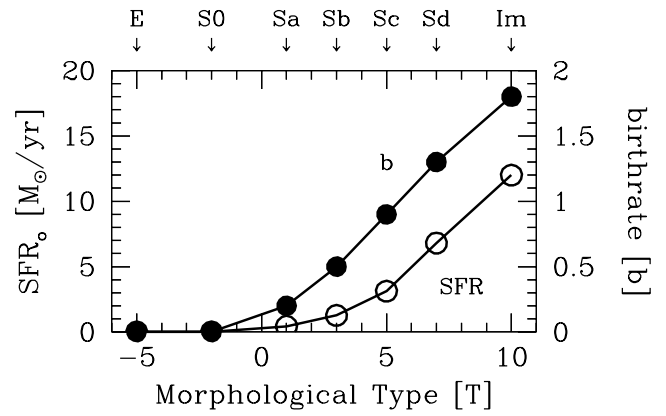


Fig. 8.—Current SFR for disk stellar populations as expected from our template models for different morphological types (left scale refers to open circles in the plot). A total mass of $10^{11} M_{\odot}$ is assumed for the galaxies. Right scale reports the mean birthrate $b = \text{SFR}_0 / \langle \text{SFR} \rangle$ according to Table 3 (*filled circles*).

extensive data samples of Roberts & Haynes (1994) and Buta et al. (1994) have been used as a reference in this regard (cf. Fig. 7).

A slightly subsolar mean metallicity (i.e., $\langle [\text{Fe}/\text{H}] \rangle = -0.5$ dex) is assumed for the disk stellar population. This is meant to be a representative average of the whole stellar population at the different epochs. Our choice agrees with Arimoto & Jablonka (1991), who suggest a luminosity-weighted value of $\langle [\text{Fe}/\text{H}] \rangle \simeq -0.3$ dex for their later-type galaxy models at 15 Gyr. The empirical age-metallicity calibration for the Milky Way by Edvardsson et al. (1993) also provides a value of $\langle [\text{Fe}/\text{H}] \rangle = -0.47$ dex when averaging on current stellar age. The conclusions of § 2.2 assure us, however, that metallicity is not a critical parameter for model predictions as far as UV evolution is concerned.

Table 3 gives a global summary of the adopted distinctive parameters for the different Hubble types at 15 Gyr (cf. also Table 1 of Massarotti et al. 2001a for a synopsis with the output of other synthesis codes). Figure 8 displays the calibration of b versus de Vaucouleurs’ “T” morphological type, and the current disk SFR expected for template galaxies of total mass $M_{\text{tot}} = 10^{11} M_{\odot}$. These results consistently compare with the empirical estimate of Kennicutt, Tamblyn, & Congdon (1994).

TABLE 3
DISTINCTIVE PARAMETERS FOR 15 GYT SYNTHESIS MODELS

Hubble Type	b^a	η	S/T^b	$M_{\text{disk}}/M_{\text{tot}}$	M/L_{bol}^c	$[\text{Fe}/\text{H}]^d$	$B-V$
S0.....	0.0	1.0	0.80	0.17	7.09	-0.10	0.90
Sa.....	0.2	0.8	0.55	0.28	5.60	-0.22	0.75
Sb.....	0.5	0.5	0.35	0.38	4.15	-0.32	0.63
Sc.....	0.9	0.1	0.18	0.52	2.73	-0.41	0.53
Sd.....	1.3	-0.3	0.05	0.78	1.66	-0.48	0.47
Irr.....	1.8	-0.8	0.00	1.00	1.11	-0.50	0.43

^a Disk stellar birthrate, $b = \text{SFR}_0 / \langle \text{SFR} \rangle$.

^b $S/T = L(\text{spheroid})/L(\text{tot})$ in bolometric.

^c Bolometric ratio for the whole model galaxy.

^d Luminosity-weighted metallicity of the global model from the bolometric partition.

TABLE 4
UV LUMINOSITY EVOLUTION FOR E GALAXIES

Age (Gyr)	U_{16-B}	U_{20-B}	U_{28-B}	$U-B$	$\log L_B$	$\log L_{\text{bol}}$
1.0.....	6.68	3.76	2.34	1.05	30.01	45.29
2.0.....	8.90	5.22	2.82	1.16	29.72	45.06
4.0.....	10.34	6.31	2.89	1.27	29.44	44.83
5.0.....	10.41	6.48	2.91	1.30	29.35	44.76
6.0.....	10.25	6.72	2.97	1.33	29.27	44.70
8.0.....	9.95	7.15	3.08	1.38	29.15	44.61
10.0.....	9.65	7.57	3.22	1.41	29.06	44.53
12.5.....	9.12	7.74	3.32	1.45	28.97	44.46
15.0.....	8.66	7.81	3.41	1.47	28.90	44.40

NOTE.—Colors are in AB scale, including Johnson $U-B$. L_B is in ergs $\text{s}^{-1} \text{Hz}^{-1}$, while L_{bol} is in erg s^{-1} . The model is normalized to $M_{\text{tot}} = 5.0 \times 10^{11} M_{\odot}$.

3.2. Model Output

Theoretical evolution of galaxy color and luminosity, pertinent to the different Hubble morphological types, is summarized in the series of Tables 4–9. All the color entries in the tables are given in AB magnitude scale⁴ including the Johnson ($U-B$), while L_B is given in ergs $\text{s}^{-1} \text{Hz}^{-1}$ and L_{bol} in ergs s^{-1} . Total luminosity of late-type galaxy models is normalized so as to provide a disk SFR = $1 M_{\odot} \text{yr}^{-1}$ at 15 Gyr; the template elliptical (taken from Buzzoni 1995) is scaled to a total mass of $5.0 \times 10^{11} M_{\odot}$. The corresponding value of M_{tot} for the other galaxy templates is reported in each table. This value only refers to the amount of mass converted in stars (that is, $M_{\text{tot}} = \int \text{SFR} dt$) and therefore does not include residual gas. By definition, its value increases with time. Absolute bolometric magnitude can be derived from the data as $\text{Bol} = -2.5(\log L_{\text{bol}} - 33.59) + 4.72$.

A preliminary “sanity check” of our theoretical output is performed in Figure 9, which compares with the Buta et al. (1994) empirical $U-B$ locus for over 2500 local galaxies in the RC3 catalog (de Vaucouleurs et al. 1991). It should be pointed out, in this regard, that this check is not completely independent, since I have already used the Buta et al. $B-V$ distribution to constrain the SFR; this would actually

⁴ For example, $(U_{20} - B) = -2.5(\log L_{2000} - \log L_B)$ in the frequency domain according to, e.g., Oke & Schild (1970).

TABLE 5
UV LUMINOSITY EVOLUTION FOR Sa GALAXIES

Age (Gyr)	U_{16-B}	U_{20-B}	U_{28-B}	$U-B$	$\log L_B$	$\log L_{\text{bol}}$
1.0.....	2.12	2.02	1.87	0.89	29.78	44.97
2.0.....	2.13	2.13	2.05	0.94	29.53	44.77
4.0.....	2.13	2.16	2.10	0.98	29.29	44.57
5.0.....	2.13	2.16	2.11	1.00	29.22	44.51
6.0.....	2.13	2.17	2.14	1.01	29.15	44.45
8.0.....	2.14	2.17	2.17	1.03	29.05	44.37
10.0.....	2.14	2.18	2.21	1.04	28.98	44.31
12.5.....	2.14	2.18	2.23	1.05	28.90	44.24
15.0.....	2.15	2.19	2.25	1.06	28.84	44.19

NOTE.—Same entries as in Table 4, but model total mass assumes SFR = $1 M_{\odot} \text{yr}^{-1}$ or $M_{\text{tot}} = 2.26 \times 10^{11} M_{\odot}$ at 15 Gyr.

TABLE 6
UV LUMINOSITY EVOLUTION FOR Sb GALAXIES

Age (Gyr)	U_{16-B}	U_{20-B}	U_{28-B}	$U-B$	$\log L_B$	$\log L_{\text{bol}}$
1.0.....	1.73	1.68	1.67	0.84	29.27	44.44
2.0.....	1.63	1.65	1.73	0.85	29.07	44.27
4.0.....	1.56	1.60	1.71	0.86	28.89	44.11
5.0.....	1.54	1.59	1.71	0.87	28.84	44.07
6.0.....	1.53	1.58	1.71	0.87	28.79	44.03
8.0.....	1.53	1.57	1.72	0.87	28.73	43.97
10.0.....	1.52	1.57	1.74	0.87	28.68	43.93
12.5.....	1.52	1.57	1.74	0.88	28.63	43.88
15.0.....	1.52	1.57	1.75	0.88	28.59	43.85

NOTE.—Same entries as in Table 4, but model total mass assumes SFR = $1 M_{\odot} \text{yr}^{-1}$ or $M_{\text{tot}} = 7.68 \times 10^{10} M_{\odot}$ at 15 Gyr.

“recover” any further internal mechanism modulating the galaxy SED. In any case, it is comforting to see from Figure 9 that the previous $B-V$ versus S/T calibration also correctly accounts, within the internal scatter of the observations, for the $U-B$ color trend versus “T” morphological parameter.

The models given in Tables 4–9 better focus on “late” galaxy evolution, after the first Gyr of life, when low-mass stars with $M \lesssim 2.0 M_{\odot}$ dominate galaxy bolometric luminosity, and bulge and disk subsystems begin to differentiate morphology along the Hubble sequence (Larson 1975, 1976; Firmani & Tutukov 1992). Evolution is less univocally constrained at earlier epochs, where convection and mass loss via stellar winds (both depending on metallicity) play an important role in high-mass stars and affect, among other things, the luminosity partition between blue and red giant stars or the relative contribution of Wolf-Rayet stars (see Mass-Hesse & Kunth 1991; Cerviño & Mass-Hesse 1994, and especially Cerviño et al. 2001 for a quantitative assessment of these problems on the framework of stellar population synthesis).

A complementary in-depth analysis of the first 10^9 yr in star-forming galaxies has been carried out by Leitherer & Heckman (1995) and Leitherer et al. (1999). Their models take into account in some detail spectrophotometric evolution of high-mass stars in different theoretical environments, including continuous star formation and SSP evolution. A match of our synthesis models and the Leitherer et al. out-

TABLE 7
UV LUMINOSITY EVOLUTION FOR Sc GALAXIES

Age (Gyr)	U_{16-B}	U_{20-B}	U_{28-B}	$U-B$	$\log L_B$	$\log L_{\text{bol}}$
1.0.....	1.61	1.58	1.60	0.83	28.74	43.92
2.0.....	1.36	1.39	1.54	0.80	28.61	43.79
4.0.....	1.22	1.26	1.45	0.77	28.52	43.70
5.0.....	1.20	1.24	1.44	0.77	28.51	43.68
6.0.....	1.19	1.23	1.44	0.76	28.49	43.66
8.0.....	1.18	1.22	1.44	0.76	28.48	43.65
10.0.....	1.18	1.23	1.45	0.76	28.47	43.64
12.5.....	1.19	1.23	1.46	0.76	28.46	43.64
15.0.....	1.20	1.24	1.47	0.76	28.46	43.64

NOTE.—Same entries as in Table 4, but model total mass assumes SFR = $1 M_{\odot} \text{yr}^{-1}$ or $M_{\text{tot}} = 3.13 \times 10^{10} M_{\odot}$ at 15 Gyr.

TABLE 8
UV LUMINOSITY EVOLUTION FOR Sd GALAXIES

Age (Gyr)	U_{16-B}	U_{20-B}	U_{28-B}	$U-B$	$\log L_B$	$\log L_{bol}$
1.0.....	1.28	1.28	1.41	0.76	28.14	43.28
2.0.....	1.00	1.05	1.27	0.70	28.12	43.23
4.0.....	0.93	0.97	1.22	0.67	28.18	43.28
5.0.....	0.93	0.98	1.22	0.67	28.21	43.31
6.0.....	0.94	0.98	1.23	0.67	28.24	43.34
8.0.....	0.96	1.00	1.25	0.68	28.28	43.39
10.0.....	0.98	1.02	1.27	0.68	28.32	43.43
12.5.....	1.01	1.05	1.30	0.69	28.36	43.48
15.0.....	1.03	1.07	1.32	0.70	28.39	43.52

NOTE.—Same entries as in Table 4, but model total mass assumes $SFR = 1 M_{\odot} \text{ yr}^{-1}$ or $M_{tot} = 1.45 \times 10^{10} M_{\odot}$ at 15 Gyr.

put for Z_{\odot} and a Salpeter IMF is shown in Figure 10. We see that SSP evolution consistently describes early-type systems at primeval epochs, while continuous SFR accounts for late-type and irregular galaxies. It is interesting to note, in addition, that colors of both ellipticals and late-type galaxies “degenerate” in the first few Myr, that is, on a time-scale comparable to t_{min} , as expected from equation (6).

Rest-frame evolution of the ($U_{20}-B$) AB color for the different galaxy morphological types is displayed in Figure 11. Only ellipticals show a drastic color change, becoming sensibly bluer at earlier epochs; late-type systems remain on the contrary more or less the same, since they are dominated throughout by fresh star formation.

The theoretical M/L ratio at 2000 Å for model ellipticals and irregulars is explored in Figure 12. I have considered the actual total mass of the galaxies, M_{tot} , in solar units according to the previous definition, while the 2000 Å luminosity derives from Table 4 and 9 as $\log L_{2000} = \log L_B - 0.4(U_{20} - B)$. The value has been converted to solar units assuming $L_{\odot} = 2.39 \times 10^{33} \text{ erg s}^{-1} \text{ Hz}^{-1}$ for the Sun at 2000 Å, as from a Kurucz (1992) ($T_{eff}, \log g$) = (5780 K, 4.5 dex) model atmosphere. As a striking feature, note that at 2000 Å enhanced star formation makes Im galaxies nearly 4 orders of magnitude brighter than ellipticals, at comparable total mass. The role of late-type systems as powerful (and possibly dominant) contributors to the cosmic UV background has recently been emphasized by Steidel, Pettini, & Adelberger (2001)

TABLE 9
UV LUMINOSITY EVOLUTION FOR Im GALAXIES

Age (Gyr)	U_{16-B}	U_{20-B}	U_{28-B}	$U-B$	$\log L_B$	$\log L_{bol}$
1.0.....	0.42	0.48	0.80	0.50	27.21	42.16
2.0.....	0.56	0.62	0.91	0.54	27.50	42.49
4.0.....	0.70	0.75	1.03	0.58	27.80	42.82
5.0.....	0.74	0.79	1.06	0.60	27.89	42.93
6.0.....	0.77	0.82	1.09	0.61	27.97	43.01
8.0.....	0.82	0.87	1.14	0.62	28.09	43.15
10.0.....	0.86	0.91	1.17	0.64	28.18	43.25
12.5.....	0.90	0.95	1.21	0.65	28.28	43.36
15.0.....	0.93	0.98	1.23	0.66	28.35	43.44

NOTE.—Same entries as in Table 4, but model total mass assumes a SFR of $1 M_{\odot} \text{ yr}^{-1}$ or $M_{tot} = 0.83 \times 10^{10} M_{\odot}$ at 15 Gyr.

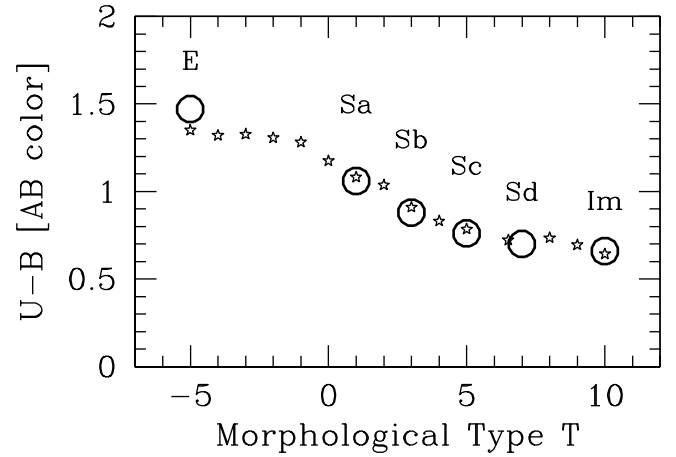


FIG. 9.—Mean observed locus for RC3 galaxies of different morphological type (*stars*) according to Buta et al. (1994), compared with 15 Gyr galaxy templates (*large open circles*). The Johnson $U-B$ color is in AB magnitude scale. Data have been originally corrected for Galaxy and internal average reddening. The typical internal scatter of the observed points is ± 0.1 mag.

and Bianchi, Cristiani, & Kim (2001) through their study of Lyman-break galaxies.

4. COMPARISON WITH UV OBSERVATIONS

Because of the intrinsic physical limits of atmosphere absorption, a study of local galaxies below 3500 Å perforce relies on a quite scanty set of data, mainly from *IUE* observations and balloon-borne missions. The work of Donas et al. (1987), collecting 2000 Å photometry for 149 mainly late-type galaxies from the SCAP 2000 balloon-borne mission, provides an important reference in this regard. Despite the large uncertainties in the original flux calibration and

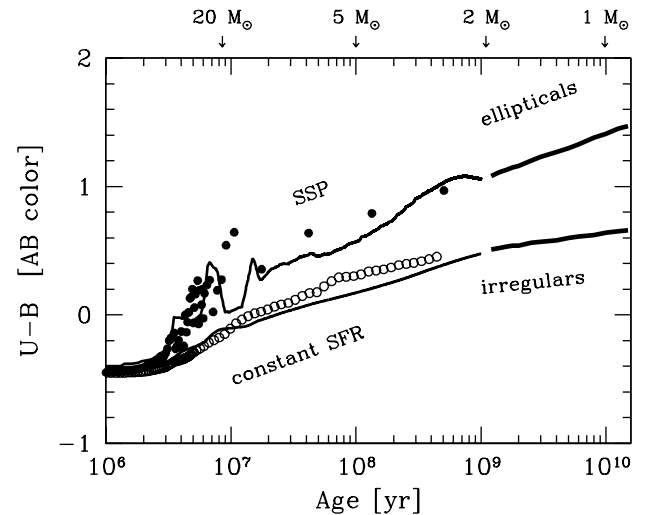


FIG. 10.—Theoretical $U-B$ colors (in AB magnitude scale) for primeval galaxies with continuous star formation (“bluer” models) and SSP evolution (“redder” models). Models with Z_{\odot} and Salpeter IMF from Leitherer & Heckman (1995) (*open and filled circles*) and Leitherer et al. (1999) (*thin solid lines*) are compared with our reference templates for E and Im galaxies (*thick solid lines*; for $t \geq 1$ Gyr). The SSP evolution consistently matches early-type systems at later epochs, while a constant SFR suitably describes late-type and irregular galaxies. The SSP TO stellar mass at different epochs is reported on the top scale, according to eq. (3).

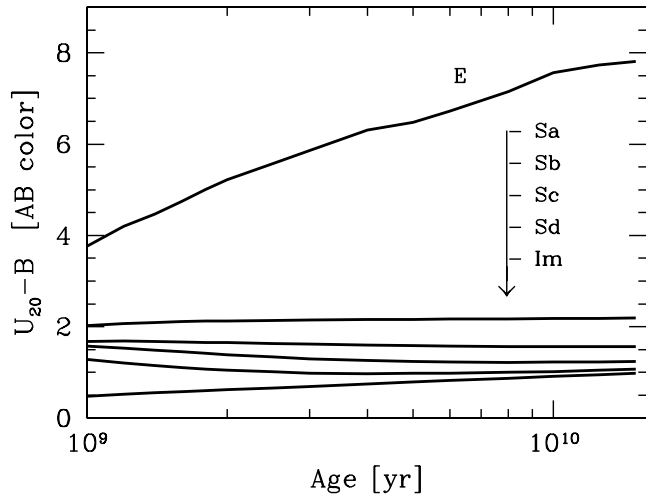


FIG. 11.—Theoretical rest-frame evolution of the $(U_{20} - B)$ AB color for model galaxies of different morphological types.

the somewhat heterogeneous match between U_{20} and (external) B photometry, a comparison with our model predictions can be attempted in Figure 13. The original data have been corrected for Milky Way extinction, relying on the Burstein & Heiles (1984) reddening map to estimate the color excess for each galaxy in the sample. According to Seaton (1979), the reddening vector is $E(U_{20} - B)/E(B - V) = 4.63$, as displayed in the figure.

Three main features are worth attention in the plot. (1) The data distribution spans a wider range in $B - V$, with “blue” and “red” outliers with respect to the 15 Gyr late-type model sequence. (2) The “thickness” of the $U_{20} - B$ data distribution exceeds the internal photometric error [reportedly $\sigma(U_{20} - B) = \pm 0.5$ mag], reaching a dispersion of ± 0.93 mag for Sa–Sb types and ± 0.65 mag for later type spirals and irregulars, as indicated by Donas et al. (1987). (3) The observations tend to be ~ 0.5 mag “redder” in $U_{20} - B$ than the late-type model sequence with $M_{\text{up}} = 120 M_{\odot}$.

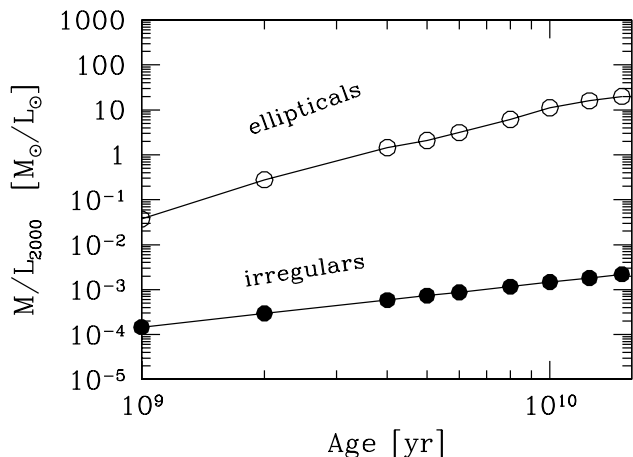


FIG. 12.—Expected evolution of the galaxy M/L ratio at 2000 \AA for the model ellipticals and irregulars, according to the data in Table 4 and 9, respectively. Both mass and luminosity are in solar units. A solar reference luminosity $L_{\odot} = 2.39 \times 10^{33} \text{ erg s}^{-1}$ is assumed at 2000 \AA from the Kurucz (1992) model atmospheres.

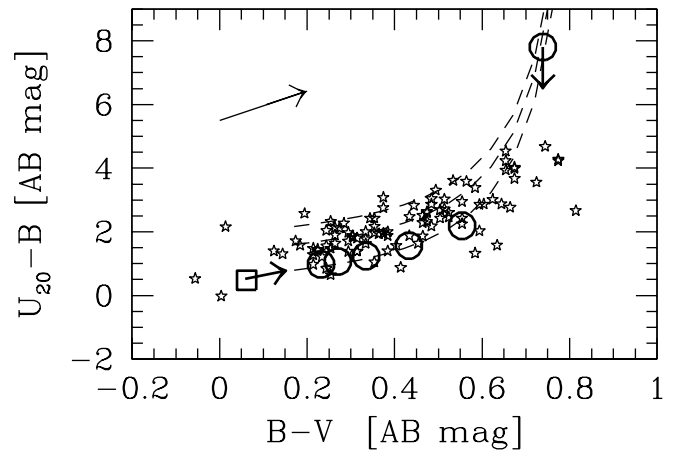


FIG. 13.—Two-color diagram of the 149 late-type galaxies in the Donas et al. (1987) sample (*stars*). Large open circles show the locus for 15 Gyr template galaxies along the sequence $\text{Im} \rightarrow \text{E}$, in the sense of increasing $B - V$. The Im model at 1 Gyr is also displayed (*large open square*). Reference models assume a Salpeter IMF with $M_{\text{up}} = 120 M_{\odot}$. The effect of residual star formation in the early-type templates is indicated by the vertical arrow on the E model. A change in the IMF upper cutoff mass for M_{up} to 80 and $60 M_{\odot}$, in the sense of “reddening” $U_{20} - B$, is explored by the dashed curves. All the colors in the plot are in AB magnitude scale. Galaxy reddening is accounted for in the original observations. The reddening vector at the top left is from Seaton (1979). The typical error bar for the UV data is ± 0.5 mag on $U_{20} - B$.

A careful analysis of the data shows that the three blue outliers [i.e., those galaxies with $(B - V) \sim 0$ in Fig. 13] are all Im systems ($T = 9\text{--}10$) with active star formation. Their integrated colors are consistent with a bulk of early-type stars (i.e., of spectral type A5 V or earlier) and therefore indicate a younger age. This is confirmed by a better fit with our 1 Gyr Im model, as reported in the figure. On the other hand, the five “red” outliers [i.e., those with $(B - V) \gtrsim 0.7$ in the plot] are all early-type or bulge-dominated systems, and are in fact “bluer” outliers when compared with the $U_{20} - B$ color of the early-type template models. These data could easily be accounted for by the E/S0 templates considering a weak ($\sim 0.2 M_{\odot} \text{ yr}^{-1}$) residual star formation instead of a plain SSP evolution (as assumed in our calculations; cf. Table 3). Although also marginally detectable in the $U - B$ plot (cf. Fig. 9), this feature more sensibly affects the 2000 \AA luminosity by changing the UV versus optical relative emission of the galaxies. In this sense, it is important to stress that UV colors of our E/S0 models should be taken as redder (upper) limits, as indicated in Figure 13.

Concerning point 2, Donas et al. (1987) ascribe most of the observed $U_{20} - B$ scatter to intrinsic galaxy-to-galaxy SFR variations. As expected, the effect should magnify at UV wavelengths, compared for example to the $B - V$ scatter. According to equation (6), the intrinsic $U_{20} - B$ distribution implies a SFR dispersion of over a factor of 2 among galaxies of the same morphological type. Table 3 helps in translating this effect in terms of $B - V$ variation. By doubling the disk birthrate, for example between the Sc and the Im template, we have a change of $\Delta(B - V) = 0.1$ mag in the galaxy integrated color; this leads to a slope of roughly $\Delta(U_{20} - B)/\Delta(B - V) \sim 7$ for the star formation “color vector” of late-type systems.

As a final point in our discussion, the “redder” offset of the $U_{20} - B$ color distribution with respect to the model sequence is open to different explanations (apart from the

comparable internal uncertainty in the U_{20} photometric zero-point of the observations). According to Table 2, a lower UV emission can be achieved either by decreasing the IMF upper cutoff or with a steeper IMF slope (that is, assuming a dwarf-dominated stellar population); alternatively, we should call for a systematically lower stellar birth-rate in the galaxies. In any case, the required change both in the IMF slope and in the current SFR would also lead to an exceedingly redder $B-V$ (Buzzoni 1989), while a lower value for M_{up} could better match the data by selectively reducing the 2000 Å emission alone, as shown in Figure 13.

A further and possibly crucial issue in this regard, however, is the galaxy internal extinction; the presence of dust would in fact act in the sense of a systematic bias toward redder UV colors. According to the Calzetti (1999) attenuation law, we obtain a color vector $E(U_{20} - B)/E(B - V) = 3.70$, so that a typical (internal) color excess $E(B - V) \sim 0.1$ mag could fairly account for the observations.

4.1. Dust and UV Absorption

Our models for galaxy spectral evolution do not explicitly include dust absorption. Its effect on galaxy SED is in the sense of suppressing UV emission and enhancing infrared luminosity, as a consequence of the thermalization process. In addition to stellar extinction, when considering external galaxies we should also account for the contribution of grain scattering, as well as the geometry of dust distribution and its partition between diffuse and “clumpy” phases. While scattering could sensibly alleviate the UV extinction (Bruzual, Magris, & Calvet 1988; Witt, Thronson, & Capuano 1992), a prevailing presence of dust segregated in interstellar clouds would act in the opposite sense (Calzetti, Kinney, & Storchi-Bergmann 1994; Kuchinski et al. 1998).

A direct way to probe dust attenuation in the galaxy SED is to evaluate the flattening of the spectral slope at short wavelength, assuming $L(\lambda) \propto \lambda^\beta$ (Kinney et al. 1993). In agreement with Leitherer et al. (1999) calculations, our dust-free models predict for late-type galaxies a value of $\beta \sim -2.4$ in the wavelength range 1600–2800 Å (cf. Tables 5–9). This should be regarded as a lower limit to the observations, since β will in general increase (up to positive values) in the presence of dust absorption. Note, by the way, that the spectral slope β is basically equivalent to a measure of the AB color in the relevant wavelength range. From the U_{16} and U_{28} AB magnitudes we have, for instance, $\beta = 1.65(U_{16} - U_{28}) - 2$.⁵

The spectral slope for local galaxies along the whole Hubble morphological type can be probed relying on the catalog of Rifatto, Longo, & Capaccioli (1995). These authors collected homogeneous data for a wide sample of 400 galaxies, mainly from the *IUE* database, reporting magnitudes in three photometric bands at 1650, 2500, and 3150 Å. Although not perfectly coincident with our wavelength range, a consistent estimate of β can be obtained for a total of 161 galaxies from the 1650 and 2500 Å magnitudes. In this regard, I preferred not to extrapolate the data to my 1600–2800 Å interval, since only a few galaxies in the

⁵ By definition, $\beta = \Delta \log F(\lambda)/\Delta \log \lambda$ and $\log F(\lambda) = \log F(\nu) - 2 \log(\lambda/c)$. Replacing the AB color definition, $C = -2.5 \Delta \log F(\nu)$, we finally obtain $\beta = -(0.4/\Delta \log \lambda) C - 2$, where $\Delta \log \lambda$ is the logarithm of the wavelength baseline on which I compute C .

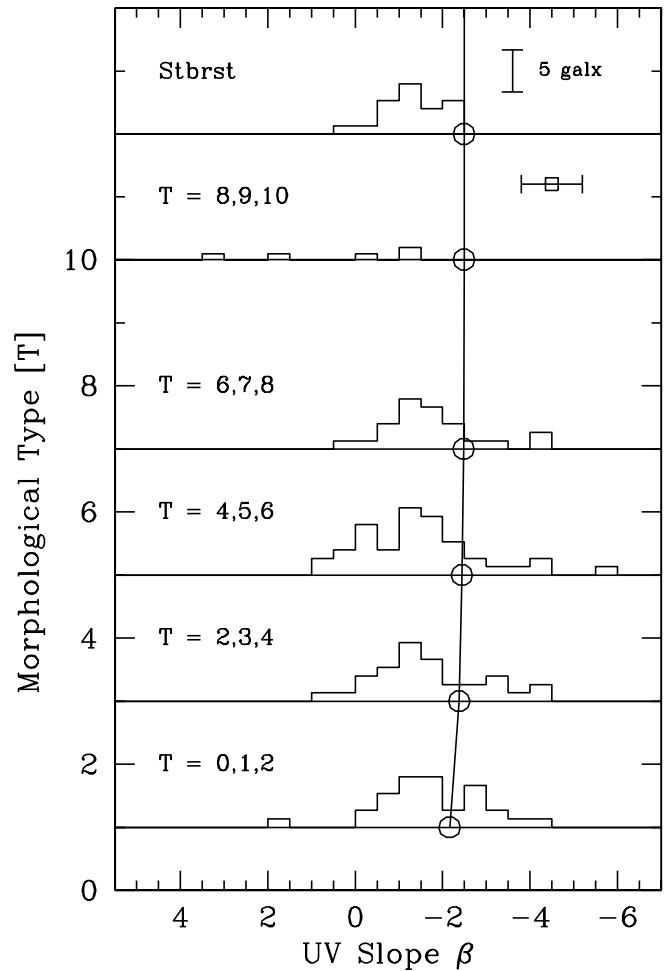


FIG. 14.—Observed distribution of the UV spectral slope, $\beta = \Delta \log L(\lambda)/\Delta \log \lambda$, for 19 starburst galaxies from Gordon et al. (1997) (top panel) and 93 spirals and irregulars ($T \geq 0$) from the *IUE* catalog of Rifatto et al. (1995). The latter sample has been grouped in five bins according to the morphological parameter T , as labeled in the different panels. Only the Gordon et al. data have been originally corrected for Galaxy reddening. Open circles and the solid line mark the theoretical lower limit to β according to our 15 Gyr template models (i.e., $\beta = -2.4$). The reddening vector is $\Delta\beta/E(B - V) = 3.1$ according to Seaton (1979), while internal attenuation is $\Delta\beta/E(B - V) = 4.5$ following Calzetti (1999). The typical uncertainty in the observed UV slope is $\sigma(\beta) \sim \pm 0.7$ for Rifatto et al. (as displayed top right in the plot) and $\sigma(\beta) \sim \pm 0.25$ for the Gordon et al. galaxies.

Rifatto et al. (1995) catalog have confident observations at 3150 Å, and this would have drastically reduced the useful sample for my analysis. Figure 14 summarizes the observed β distribution for the late-type galaxy subsample (93 galaxies in total). To study a possible trend with galaxy morphology, data have been grouped in five bins according to the de Vaucouleurs’ T parameter, as indicated in the plots. In addition to the Rifatto et al. (1995) sample, the figure also includes the relevant results for 19 starburst galaxies from Gordon, Calzetti, & Witt (1997) with complete seven-band photometry between 1250 and 2895 Å; this allowed a confident estimate of β at the nominal wavelength range of the models.

As a general trend, note from Figure 14 that galaxy distribution always peaks, on average, at flatter UV slopes (i.e., $\beta > -2.4$) compared to our theoretical lower limit; this indicates that some intervening absorption is systematically

affecting the observations, with starburst and later type galaxies (Sd/Im) marginally more obscured than Sa/Sb systems. The effect of dust reddening seems to exceed the internal uncertainty of the data, that is, $\sigma(\beta) \simeq \pm 0.7$ for Rifatto et al. (1995) and $\sigma(\beta) \simeq \pm 0.25$ for Gordon et al. (1997). The Gordon et al. (1997) data were originally corrected for the average Galactic extinction, and they better track the net effect of internal dust absorption. This is not the case for the Rifatto et al. (1995) sample, where the UV flattening is a sum of both internal galaxy attenuation and Milky Way extinction.

According to the Seaton (1979) extinction law, the expected reddening vector for the 1600–2800 Å UV slope is $\Delta\beta/E(B-V) = 3.1$, while the Calzetti (1999) attenuation law suggests $\Delta\beta/E(B-V) = 4.5$. An average flattening of $\Delta\beta \sim 1$, as shown by the data, therefore implies an internal color excess of $E(B-V) \lesssim 0.2$ mag, consistent with the Donaş et al. (1987) data. This is about a 2 mag extinction at 1600 Å, according to Calzetti (1999).

4.2. Dust Absorption and High-Redshift Galaxy Evolution

The role of dust has raised to a central issue in the current cosmological debate, given its importance for a fair determination of the cosmic SFR through the UV observation of high-redshift galaxies (Hughes et al. 1998; Steidel et al. 1999; Massarotti et al. 2001b; Hopkins et al. 2001).

Generally speaking, a large fraction of residual gas, such as in primeval galaxies, should call for a *low* amount of dust. The latter is in fact a natural result of stellar evolution (mass loss and supernova events actually supply the basic ingredients for grain formation), and should therefore *follow* star formation not *precede* it. As a matter of fact, however, young starbursters certainly appear to be more dust-rich than old quiescent ellipticals (Calzetti et al. 1994). The association of greater quantities of dust with strongly star-forming galaxies may perhaps be due to a shorter timescale for dust than for star formation, or more likely to a feedback process, by which starbursts preferentially occur in dense gas/molecular clouds already heavily contaminated by dust.

Both of these arguments point to a tight relationship between dust absorption (and its induced IR emission) and galaxy UV luminosity, as found by Meurer, Heckman, & Calzetti (1999); apparently, this correlation is already in place at high redshift, as demonstrated by Adelberger & Steidel (2000). A dominant contribution of the UV-selected galaxy population to the IR cosmic background is also in line with the results of Massarotti et al. (2001b), who fully reconcile the SCUBA estimates for SFR density at high z (Barger, Cowie, & Richards 2001) with the Hubble Deep Field optical observations.

An important point that one should bear in mind, however, is that dust comes from cumulative processes inside galaxies, and its content should generally increase with time; contrary to the observations, this would predict more heavily obscured systems at the present time. In order to break this apparent dichotomy we need to “split,” at some point of galaxy evolution, the distribution of the luminous matter (i.e., stars) and dust. The case of our own Galaxy might be explanatory in this sense.

Because of a higher velocity dispersion and supernova shock waves, young O-B associations leave parent molecular clouds and spread their B stars across the disk on a time-

scale of some 10^7 yr, a value comparable to the lifetime of stars of 5–10 M_{\odot} (see, in this regard, the classical work of Becker & Fenkart 1963, or the recent contribution of Hoogerwerf, de Bruijne, & de Zeeuw 2001). If this is also the case for external galaxies, then an increasing fraction of luminous matter would quickly escape the regions of harder and “clumpy” dust absorption (Calzetti 1999) moving toward a milder and “scattered” dust environment (Bruzual et al. 1988). This scenario would consistently explain, among other things, why dust attenuation seems to affect gas clouds more severely than stars even in starburst galaxies (Calzetti et al. 1994).

5. SUMMARY AND CONCLUSIONS

In this paper I have explored some relevant features dealing with the UV luminosity evolution of primeval galaxies, in view of a direct application to high-redshift studies. This has been done via a new set of evolutionary population synthesis models that provide reference templates for different galaxy morphological types. Theoretical SEDs for late- and early-type systems have been derived, together with detailed luminosity evolution at 1600, 2000, and 2800 Å.

As expected, the galaxy UV luminosity below 3000 Å is largely dominated by the high-mass stellar component, and the distinctive properties of the integrated SED are nearly independent of both the total mass of the galaxy and its past star formation history. At every age, this leads to a direct relationship between galaxy UV luminosity and actual SFR (cf. eq. [6] and Fig. 4).

Because of a faster evolution of the bulge stellar population (basically a SSP with $L_{UV} \propto t^{-\gamma}$ and $\gamma \geq 1$), the high-redshift ancestors of present-day spirals should appear as sharply nucleated objects displaying scarce or no morphological structure. In addition, early galaxy evolution ($t \leq 1$ Gyr) could also display some color “degeneracy” in the UV range (cf. Fig. 10), loosing any clear relationship between photometric properties and galaxy morphology along the Hubble sequence. This effect should not be neglected for its possible importance in a fair sampling of the galaxy population at high redshift (Buzzoni 1998).

The claimed role of late-type systems as prevailing contributors to the cosmic UV background is reinforced by our results; at 2000 Å Im irregulars are found in fact to be nearly 4 orders of magnitude brighter than ellipticals, per unit luminous mass (cf. Fig. 12).

The UV wavelength range is especially sensitive to dust absorption; this problem should be properly assessed in high-redshift studies. The SED of local starburst and late-type galaxies shows clear evidence of some intrinsic reddening systematically affecting galaxies in their active star-forming stage. The amount of luminosity extinction for these objects sensibly depends on the assumed dust environment and grain properties, but it may be as high as 2 mag at 1600 Å in the most typical cases.

Dust is expected to cumulate along the galaxy lifetime, so that the M_{dust}/L ratio should increase more than linearly with time for both spirals and ellipticals. However, the apparent lack of strong reddening in old quiescent systems at the present time indicates that even in the UV range most of the luminous contribution comes from relatively unabsorbed stars. This would call for some evolution in the dust environment, where a pristine “clumpy” extinction regime, such as in the Calzetti et al. (1994) scheme, would quickly

turn into a diffuse “scattered” reddening, as in the Bruzual et al. (1988) models.

It is a pleasure to thank the anonymous referee for his/her important suggestions that greatly helped in tuning the

original discussion. Emanuele Bertone is acknowledged for his precious help with the calculation of the Kurucz model atmospheres, used in this work. This project received partial financial support from the Italian MURST under grants COFIN98 02-013 and COFIN00 02-016.

REFERENCES

- Adelberger, K. L., & Steidel, C. C. 2000, *ApJ*, 544, 218
 Allen, C. W. 1973, *Astrophysical Quantities* (London: Athlone)
 Arimoto, N., & Jablonka, P. 1991, *A&A*, 249, 374
 Barger, A. J., Cowie, L. L., & Richards, E. A. 2000, *AJ*, 119, 2092
 Becker, S. A. 1981, *ApJS*, 45, 475
 Becker, W., & Fenkart, R. 1963, *Z. Astrophys.*, 56, 257
 Bianchi, S., Cristiani, S., & Kim, T. S. 2001, *A&A*, 376, 1
 Bressan, A., Fagotto, F., Bertelli, G., & Chiosi, C. 1993, *A&AS*, 100, 647
 Bruzual, G. A., & Charlot, S. 1993, *ApJ*, 405, 538
 Bruzual, G. A., Magris, G. C., & Calvet, N. 1988, *ApJ*, 333, 673
 Burstein, D., Bertola, F., Buson, L., Faber, S. M., & Lauer, T. R. 1988, *ApJ*, 328, 440
 Burstein, D., & Heiles, C. 1984, *ApJS*, 54, 33
 Buta, R., Mitra, S., de Vaucouleurs, G., & Corwin, H. G., Jr. 1994, *AJ*, 107, 118
 Buzzoni, A. 1989, *ApJS*, 71, 817
 ———. 1995, *ApJS*, 98, 69
 ———. 1998, in *IAU Symp. 183, Cosmological Parameters and Evolution of the Universe*, ed. K. Sato (Dordrecht: Kluwer), 134
 ———. 2001, in *The Link between Stars and Cosmology*, ed. M. Chavez, et al. (Dordrecht: Kluwer), in press (astro-ph/0107273)
 Cacciari, C., Fusi Pecci, F., Bragaglia, A., & Buzzoni, A. 1995, *A&A*, 301, 684
 Calzetti, D. 1999, *Mem. Soc. Astron. Italiana*, 70, 715
 Calzetti, D., Kinney, A. L., & Storchi-Bergmann, T. 1994, *ApJ*, 429, 582
 Castellani, V., Chieffi, A., & Straniero, O. 1990, *ApJS*, 74, 463
 Cerviño, M., & Mass-Hesse, J. M. 1994, *A&A*, 284, 749
 Cerviño, M., Valls-Gabaud, D., Luridiana, V., & Mas-Hesse, J. M. 2002, *A&A*, 381, 51
 Connolly, A. J., Szalay, A. S., Dickinson, M., Subbarao, M. U., & Brunner, R. J. 1997, *ApJ*, 486, L11
 de Vaucouleurs, G., de Vaucouleurs, A., Corwin, H. G., Jr., Buta, R. J., Paturel, G., & Fouque, P. 1991, *Third Reference Catalog of Bright Galaxies* (Heidelberg: Springer)
 Donas, J., Deharveng, J. M., Laget, M., Milliard, B., & Huguenin, D. 1987, *A&A*, 180, 12
 Edvardsson, B., Andersen, J., Gustafsson, B., Lambert, D. L., Nissen, P. E., & Tomkin, J. 1993, *A&A*, 275, 101
 Fagotto, F., Bressan, A., Bertelli, G., & Chiosi, C. 1994, *A&AS*, 105, 29
 Fioc, M., & Rocca-Volmerange, B. 1997, *A&A*, 326, 950
 Firmani, C., & Tutukov, A. V. 1992, *A&A*, 264, 37
 Gavazzi, G. 1993, *ApJ*, 419, 469
 Gordon, K. D., Calzetti, D., & Witt, A. N. 1997, *ApJ*, 487, 625
 Greggio, L., & Renzini, A. 1990, *ApJ*, 364, 35
 Hoogerwerf, R., de Bruijne, J. H. J., & de Zeeuw, P. T. 2001, *A&A*, 365, 49
 Hopkins, A. M., Connolly, A. J., Haarsma, D. B., & Cram, L. E. 2001, *AJ*, 122, 288
 Hughes, D. H., et al. 1998, *Nature*, 394, 241
 Kennicutt, R. C., Jr. 1998, *ARA&A*, 36, 189
 Kennicutt, R. C., Jr., Tamblyn, P., & Congdon, C. W. 1994, *ApJ*, 435, 22
 Kent, S. M. 1985, *ApJS*, 59, 115
 Kinney, A. L., Bohlin, R. C., Calzetti, D., Panagia, N., & Wyse, R. F. G. 1993, *ApJS*, 86, 5
 Kuchinski, L. E., Terndrup, D. M., Gordon, K. D., & Witt, A. N. 1998, *AJ*, 115, 1438
 Kurucz, R. 1992, in *IAU Symp. 149, The Stellar Populations of Galaxies*, ed. A. Renzini & B. Barbuy (Dordrecht: Kluwer), 225
 Lanzetta, K. M., Yahil, A., & Fernández-Soto, A. 1996, *Nature*, 381, 759
 Larson, R. B. 1975, *MNRAS*, 173, 671
 ———. 1976, *MNRAS*, 176, 31
 Larson, R. B., & Tinsley, B. M. 1978, *ApJ*, 219, 46
 Lattanzio, J. 1991, *ApJS*, 76, 215
 Leitherer, C., & Heckman, T. M. 1995, *ApJS*, 96, 9
 Leitherer, C., Schaerer, D., Goldader, J. D., González Delgado, R. M., Robert, C., Foo Kune, D., de Mello, D. F., Devost, D., & Heckman, T. M. 1999, *ApJS*, 123, 3
 Lilly, S. J., Le Fèvre, O., Hammer, F., & Crampton, D. 1996, *ApJ*, 460, L1
 Madau, P., Pozzetti, L., & Dickinson, M. 1998, *ApJ*, 498, 106
 Mas-Hesse, J. M., & Kunth, D. 1991, *A&AS*, 88, 399
 Massarotti, M., Iovino, A., & Buzzoni, A. 2001a, *A&A*, 368, 74
 ———. 2001b, *ApJ*, 559, L105
 Massarotti, M., Iovino, A., Buzzoni, A., & Valls-Gabaud, D. 2001c, *A&A*, 380, 425
 Meurer, G. R., Heckman, T. M., & Calzetti, D. 1999, *ApJ*, 521, 64
 Oke, J. B., & Schild, R. E. 1970, *ApJ*, 161, 1015
 Renzini, A., & Buzzoni, A. 1986, in *Spectral Evolution of Galaxies*, ed. C. Chiosi & A. Renzini (Dordrecht: Reidel), 195
 Rifatto, A., Longo, G., & Capaccioli, M. 1995, *A&AS*, 114, 527
 Roberts, M. S., & Haynes, M. P. 1994, *ARA&A*, 32, 115
 Scalo, J. M. 1986, *Fundam. Cosmic Phys.*, 11, 1
 Schaller, G., Schaerer, D., Meynet, G., & Maeder, A. 1992, *A&AS*, 96, 269
 Seaton, M. J. 1979, *MNRAS*, 187, 73P
 Steidel, C. C., Adelberger, K. L., Giavalisco, M., Dickinson, M., & Pettini, M. 1999, *ApJ*, 519, 1
 Steidel, C. C., Pettini, M., & Adelberger, K. L. 2001, *ApJ*, 546, 665
 Vandenberg, D. A. 1985, *ApJS*, 58, 711
 Williams, R. E., et al. 1996, *AJ*, 112, 1335
 Witt, A. N., Thronson, H. A., Jr., & Capuano, J. M., Jr. 1992, *ApJ*, 393, 611
 Yi, S., Lee, Y., Woo, J., Park, J., Demarque, P., & Oemler, A., Jr. 1999, *ApJ*, 513, 128